J Physiol 592.21 (2014) pp 4657–4676

The Journal of Physiology

Voltage- and ATP-dependent structural rearrangements of the P2X2 receptor associated with the gating of the pore

Batu Keceli[1] and Yoshihiro Kubo[1,2]

[1] *Division of Biophysics and Neurobiology, Department of Molecular Physiology, National Institute for Physiological Sciences, Okazaki, Aichi 444-8585, Japan*

[2] *Department of Physiological Sciences, The Graduate University for Advanced Studies (SOKENDAI), School of Life Science, Hayama, Kanagawa 240-0155, Japan*

Key points

- We previously reported that the ATP receptor channel P2X2 shows gating which depends not only on ATP but also on membrane voltage, in spite of the absence of a canonical voltage sensor.
- The purpose of the present study was to capture the structural rearrangements of P2X2 associated with voltage- and ATP-dependent gating.
- Cysteine residues were introduced by mutation at Asp315 and Ile67 in the linker region located between the ATP binding site and the channel pore. We analysed the modification rate of cysteine residues by Cd^{2+} by recording current under two-electrode voltage clamp using *Xenopus* oocytes.
- Two cysteine residues at 315 and 67 were bridged by Cd^{2+} resulting in current decline, and the speed of modification was faster at hyperpolarized than at depolarized potential, and also faster in the presence than in the absence of ATP.
- The bridging by Cd^{2+} between 315 and 67 was not intra- but inter-subunit.
- The results demonstrate the structural rearrangements in the linker region of P2X2 associated with voltage- and ATP-dependent gating of the pore.

Abstract P2X2 is an extracellular ATP-gated cation channel which has a voltage-dependent gating property even though it lacks a canonical voltage sensor. It is a trimer in which each subunit has two transmembrane helices and a large extracellular domain. The three inter-subunit ATP binding sites are linked to the pore forming transmembrane (TM) domains by β-strands. We analysed structural rearrangements of the linker strands between the ATP binding site and TM domains upon ligand binding and voltage change, electrophysiologically in *Xenopus* oocytes, using mutants carrying engineered thiol-modifiable cysteine residues. (1) We demonstrated that the double mutant D315C&I67C (at β-14 and β-1, respectively) shows a 2- to 4-fold increase in current amplitude after treatment with a reducing reagent, dithiothreitol (DTT). Application of the thiol-reactive metal Cd^{2+} induced current decline due to bond formation between D315C and I67C. This effect was not observed in wild type (WT) or in single point mutants. (2) Cd^{2+}-induced current decline was analysed in hyperpolarized and depolarized conditions with different pulse protocols, and also in the presence and absence of ATP. (3) Current decline induced by Cd^{2+} could be clearly observed in the presence of ATP, but was not clear in the absence of ATP, showing a state-dependent modification. (4) In the presence of ATP, Cd^{2+} modification was significantly faster in hyperpolarized than in depolarized conditions, showing voltage-dependent structural rearrangements of the linker strands. (5) Experiments using tandem trimeric constructs (TTCs) with controlled number and position of mutations in the trimer showed that the bridging by Cd^{2+} between 315 and 67 was not intra- but inter-subunit. (6) Finally, we performed similar

DOI: 10.1113/jphysiol.2014.278507

analyses of a pore mutant T339S, which makes the channel activation voltage insensitive. Cd^{2+} modification rates of T339S were similar in hyperpolarized and depolarized conditions. Taking these results together, we demonstrated that structural rearrangements of the linker region of the P2X2 receptor channel are induced not only by ligand binding but also by membrane potential change.

(Received 3 June 2014; accepted after revision 11 August 2014; first published online 28 August 2014)
Corresponding authors B. Keceli: Y. Kubo: Department of Molecular Physiology, National Institute for Physiological Sciences, Okazaki, Aichi 444-8585, Japan. Email: ykubo@nips.ac.jp

Abbreviations ACh, acetylcholine; ATP, adenosine triphosphate; D315C, a mutant of P2X2 in which aspartate residue at 315 is mutated to cysteine residue; D315C&I67C, a double mutant of D315C and I67C; DTT, dithiothreitol; *G–V*, conductance–voltage relationship; I67C, a mutant of P2X2 in which isoleucine residue at 67 is mutated to cysteine residue; MR, modification rate; SEM, standard error of means; TM, transmembrane; TTC, tandem trimeric construct; USER, uracil-specific excision reagents; WT, wild type.

Introduction

P2X receptors are extracellular ATP-gated cation channels which are widely distributed in various physiological systems (Khakh, 2001; North, 2002; Khakh & North, 2006, 2012). P2X receptors have a trimeric structure in which each subunit has two transmembrane domains (TM1 and TM2) and a large extracellular domain. Crystal structures in both closed and open states (Kawate *et al.* 2009; Hattori & Gouaux, 2012) revealed that three extracellular inter-subunit ATP binding sites are located approximately 40 Å distant from the membrane and linked to the pore forming TM helices by β-strands (Fig. 1*A* and *B*). Comparison of the closed and open state structures shows that ATP binding causes an apparent widening of the pore formed by steeply angled TM2 helices and also separation and bending of linker strands, which might reflect the transmission of the ATP binding signal to the pore (Kawate *et al.* 2009; Hattori & Gouaux, 2012). However, it was reported that the open state structure in the membrane could be different from that in the crystal (Heymann *et al.* 2013) and thus the dynamic image of the rearrangement from closed to open remains to be clarified.

Recent Cys-accessibility analyses of TM helices using thiol-reactive reagents and structural data revealed that the P2X2 receptor gate is formed by TM2 residues Ile332 and Ile341 (Li *et al.* 2010). TM1 helices, surrounding the pore forming TM2 helices, do not directly contribute to ion permeation, but evidence from recent computational and functional data suggest that TM1 domains contribute to fine-tuning of gating (Li *et al.* 2008, 2010; Jindrichova *et al.* 2009; Keceli & Kubo, 2009).

We previously showed that, in the steady state after ATP application, inward current through P2X2 gradually increases upon hyperpolarization and the conductance–voltage relationship (*G–V*) plot shifts to depolarized potentials with the increase in [ATP] (Fujiwara *et al.* 2009; Keceli & Kubo, 2009). The P2X2 channel is devoid of any secondary mechanisms such as voltage-dependent block/unblock by positively charged cations or substances, or an inactivation 'ball' mechanism (Zhou & Hume, 1998; Fujiwara *et al.* 2009; Keceli & Kubo, 2009; Kubo *et al.* 2009). Non-canonical voltage sensing mechanisms have also been reported for nicotinic acetylcholine (ACh) receptors (Charnet *et al.* 1992; Figl *et al.* 1996), muscarinic ACh receptors (Ben-Chaim *et al.* 2003, 2006), and metabotropic glutamate receptors (Ohana *et al.* 2006). The structural basis of non-canonical voltage sensing remains to be elucidated.

In this study, we primarily focused on the voltage-dependent structural rearrangements of the linker β-strands which transmit the ATP binding signal to the pore in the TM helices. To approach a dynamic image of the voltage- and [ATP]-induced rearrangements, we utilized a combined technique of mutagenesis and chemical modification. By introducing a pair of cysteine residues at Asp315 (D315) and Ile67 (I67), we identified a thiol-modifiable site in the linker domain (Fig. 1). The application of a thiol-modifying reagent, Cd^{2+}, reduced the inward current due to the formation of a –S–Cd–S– bond between the substituted cysteine residues. This effect was not observed in WT or single mutants. By taking advantage of this thiol-modifiable site, we analysed the state-dependent modifications and structural rearrangements of the linker domain in the presence/absence of ATP and in hyperpolarized/depolarized conditions.

Methods

Ethical approval

All animal experiments in this study conformed to the guidelines of the Animal Care and Use Committee of the National Institute for Physiological Sciences (Okazaki, Japan) and were performed with the approval of the committee.

In vitro mutagenesis and cRNA synthesis

A *Bam*HI–*Not*I fragment of the rat P2X2 cDNA (Brake *et al.* 1994) was subcloned into the *Sma*I site of pGEMHE. Single- and double-point mutants were made using a QuikChange site directed mutagenesis kit (Stratagene, La Jolla, CA, USA) and confirmed by DNA sequencing as described previously (Fujiwara *et al.* 2009; Keceli & Kubo, 2009). Tandem trimer constructs (TTCs), i.e. concatemers used in Fig. 8, were constructed as described previously (Keceli & Kubo, 2014). Briefly, each subunit was amplified using unique pairs of PCR primers, which had 7- to 12-nucleotide long custom-made overhangs with an intentionally introduced uracil. After PCR, this uracil was excised with USER enzyme (uracil specific excision enzyme, which is a mixture of uracil DNA glycosylase and DNA glycosylase-lyase Endo VIII from New England Biolabs, UK), which creates single stranded overhangs designed to be complementary to that of the neighboring subunit to be ligated. The pNB1u vector was digested with PacI and Nt.BbvCI to generate 8-nucleotide long overhangs. By this method, ligation of amplified subunits and vector was successfully achieved in the desired order (Nour-Eldin *et al.* 2010). The plasmid cDNA was linearized by *Nhe*I and cRNA was transcribed using mMESSAGE T7 RNA transcription kit (Ambion, Inc., Austin, TX, USA) as described previously (Fujiwara *et al.* 2009; Keceli & Kubo, 2009).

Preparation of *Xenopus* oocytes

Xenopus oocytes were surgically collected from frogs anaesthetized in water containing 0.15% tricaine. After the final collection, the frogs were killed by decapitation. Isolated oocytes were treated with collagenase (2 mg ml^{-1}; type 1; Sigma-Aldrich) for 6 h. After the treatment, oocytes of similar size at stage V were injected with 50 nl of cRNA solution as described previously (Fujiwara *et al.* 2009; Keceli & Kubo, 2009). The injected oocytes were then incubated in frog Ringer solution for 1–2 days at 17°C and then moved to 4–8°C in order to avoid very high expression levels.

Two-electrode voltage clamp recordings in *Xenopus* oocytes

Macroscopic currents were recorded from *Xenopus* oocytes under the two-electrode voltage clamp technique using an OC-725C (Warner Instruments, LLC, Hamden, CT, USA) bath clamp amplifier as described previously (Fujiwara *et al.* 2009; Keceli & Kubo, 2009). Stimulation and data acquisition were performed on a Pentium-based computer using Digidata 1322A and pCLAMP 9.2 software (Axon Instruments/Molecular Devices, Sunnyvale, CA, USA). All recordings were obtained at room temperature. Intracellular glass microelectrodes were filled with 3 M potassium acetate containing 10 mM KCl (pH 7.2), and the resistance ranged from 0.1 to 0.3 MΩ. Two Ag–AgCl pellets (Warner Instruments) were used to pass the bath current and record the bath voltage. The recording bath solution contained 95.6 mM NaCl, 1 mM $MgCl_2$, 5 mM Hepes, and 2.4 mM NaOH at pH 7.35–7.44. ATP disodium salt (Sigma-Aldrich) and other chemicals were dissolved in bath solution (pH 7.35). We set the initial bath volume as 160 μl and applied 40 μl (one-fifth of the total bath volume of 200 μl) of 5× concentrated ATP solution by pipetting. In order to maintain stable concentrations of ATP in the case of application of a second chemical without prior washing; we applied the second chemical, the thiol reactive reagent, with 1 × [ATP], the [ATP] being of one-fifth (50 μl) of a 5× concentration or one-tenth (22 μl) of a 10× concentration, when necessary. Oocytes expressing relatively low levels of P2X2 were used to achieve sufficiently accurate voltage clamp and to avoid changes in the properties of the channel due to the high expression level (Fujiwara & Kubo, 2004; Fujiwara *et al.* 2009; Keceli & Kubo, 2009). Oocytes having leak currents larger than ∼0.3 μA at −40 mV were discarded. In order to monitor the modification rates of the constructs by Cd^{2+} in hyperpolarized and depolarized conditions, two different pulse protocols were used. For the hyperpolarized condition, oocytes were clamped at a holding potential of −20 mV and repetitive hyperpolarizing step pulses to −100 mV for 500 ms were applied once every second. For the depolarized condition, the holding potential was +40 mV and hyperpolarizing step pulses were applied once every 5 s. Time lapse changes of the maximum inward current amplitudes at −100 mV were monitored.

The data from WT and the T339S pore mutant shown in Fig. 9*A* were recorded by applying a set of step pulses during the steady state about 8–10 s after agonist application. The background leak current before ATP application was measured and subtracted to isolate the ATP-induced current. Oocytes having leak currents larger than 0.3 μA at −40 mV were discarded.

Data analysis

Data were analysed using Clampfit 9.2 (Axon Instruments) and Igor Pro (WaveMetrics, Inc., Lake Oswego, OR, USA) software as described previously (Fujiwara *et al.* 2009; Keceli & Kubo, 2009).

In Fig. 4, voltage-induced activation phases before and after Cd^{2+} applications were analysed by fitting with a single exponential function.

In Fig. 5, the time constant for modification (τ) was obtained by fitting the time course of the change of the inward currents with a single exponential function (Fig. 5*C*). Then, the modification rates (MR) were

obtained from: MR = $1/(M\ (\text{mol}) \times \tau\ (\text{s}))$, where M is the concentration of the modifying reagent (Cd^{2+}) and τ is the time constant for modification (Fig. 5*E* and *F*).

In Fig. 6*E*, MRs obtained with 1 mM Cd^{2+} in various [ATP], as well as dose–response relationships for WT P2X2 at −100 mV, were plotted as a function of [ATP] in hyperpolarized and depolarized conditions and fitted with the Hill–Langmuir equation:

$$\text{MR} = \frac{\text{MR}_{\max}[\text{ATP}]^h}{\text{EC}_{50}^h + [\text{ATP}]^h} \quad \text{and} \quad I = \frac{I_{\max}[\text{ATP}]^h}{\text{EC}_{50}^h + [\text{ATP}]^h},$$

where I is the current amplitude and h is the Hill coefficient.

For analysis of the *G–V* relationship in Fig. 9*B*, the inward tail current amplitudes at −60 mV were measured and fitted with a two-state Boltzmann equation:

$$I = I_{\min} + \frac{I_{\max} - I_{\min}}{1 + e^{-\frac{ZF}{RT}(V - V_{1/2})}},$$

where $I_{\min}$ and $I_{\max}$ are the limits of the amplitudes for the fits, Z is the effective charge, $V_{1/2}$ (mV) is the half-activation voltage, F is Faraday's constant, R is the gas constant, and T is temperature in Kelvin. $I_{\min}$ here is the inward current with the largest amplitude. Normalized *G–V* relationships were fitted using the following equation:

$$G/G_{\max} = I/I_{\min} = 1 - \left(1 + e^{-ZF\left(V - V_{\frac{1}{2}}\right)/RT}\right)^{-1}(1 - I_{\max}/I_{\min}).$$

Statistical analyses

One-factor ANOVA and *post hoc* pairwise comparisons were used for multi-group comparison in Figs 2*E*, 3*E* and 8*C*. Student's *t* test was used for pairwise comparisons in Figs 4*E*, 5*D*, 6*D*, 7*C* and 9*E*. For all statistical analyses, cases of $P < 0.05$ (*) were judged as significantly different. Double and triple asterisks (** and ***) indicate $P < 0.01$ and $P < 0.001$, respectively. The values were shown as means ± standard error of means (SEM) (n).

Three dimensional structural modelling of rat P2X2

Homology modelling of rat P2X2 in the closed state and open state was performed (Keceli & Kubo, 2009) based on sequence alignment of amino acid residues 34–351 of the rat P2X2 and zebra fish P2X4 whose crystal structures have been solved (Protein Data Bank accession number 3I5D (closed state) and 4DW1 (open state); Kawate *et al.* 2009; Hattori & Gouaux, 2012), using DeepView/Swiss pdb viewer v.4.0.1 (http://www.expasy.org/spdbv/) and SWISS-MODEL (Automated Protein Modelling Server) (Arnold *et al.* 2006; Bordoli *et al.* 2009; Kiefer *et al.* 2009). The homology modelling data were used for the graphic presentations (Figs 1 and 10) made by PyMol (DeLano Scientific LLC, Palo Alto, CA, USA).

Western blotting

To confirm the inter-subunit Cys–Cys bond formation between D315C and I67C biochemically, we performed Western blotting and compared the sizes of the bands for the constructs WT, I67C, D315C, and D315C&I67C in the presence and absence of reducing reagent DTT (Fig. 2*F*). Briefly, oocytes were frozen 3–4 days after injection of cRNA. Frozen oocytes were sonicated in PBS containing protease inhibitor cocktail (Roche, Mannheim, Germany). Homogenate was centrifuged at 3000 rpm at 4°C for 10 min to remove yolk and the resultant supernatant was used as whole protein extract. The samples were mixed with SDS (+), DTT (–) or SDS (+), DTT (+) dye solution and loaded on the gel. Western blotting was performed using an affinity purified anti-P2X2 rabbit antibody (Sigma Aldrich Inc.). The region used as immunogenic corresponds to amino acids 457–472 of rat P2X2 with an additional Cys at the N-terminal end.

Results

Identification of D315C&I67C as a redox regulated channel

In order to eliminate native cysteine residues and prepare a suitable background for our experiments we initially mutated Cys9, Cys348, and Cys430 to Thr and produced 3T-WT P2X2. 3T-WT P2X2 has previously been shown to be highly similar to WT in terms of dose–response relationship (Li *et al.* 2008, 2010). As we also observed voltage-dependent gating of this construct (data not shown) to be highly similar to WT P2X2 in our previous studies (Fujiwara *et al.* 2009; Keceli & Kubo, 2009), we used this 3T-WT construct for all further experiments in this study as WT and background for additional mutations.

The oocytes expressing WT P2X2, D315C (at β-14), I67C (at β-1), or double mutant D315C&I67C were clamped at −80 mV and the response to 1 mM ATP was compared before and after application of the reducing reagent DTT (10 mM, 1 min; Fig. 2*A–D*). Compared to WT and single mutants, the double mutant D315C&I67C showed a 2- to 4-fold increase in the maximum inward current after DTT application (Fig. 2*D*). The increase in the inward current for the double mutant D315C&I67C was significantly larger than that of WT and single mutants (Fig. 2*E*; $P < 0.001$, $n = 6$–14).

The current amplitudes before normalization of the WT and mutants (mean ± SEM in μA) were as follows:

before DTT treatment, WT = 9.5 ± 1.5 (n = 11), I67C = 5.2 ± 1.2 (n = 6), D315C = 9.6 ± 2.8 (n = 8), D315C&I67C = 4.7 ± 0.7 (n = 14); after DTT treatment, D315C&I67C = 13.6 ± 2.0 (n = 14). The EC_{50} values of ATP (mean ± SEM in μM) were as follows: WT = 13.1 ± 1.5 (n = 7), I67C = 24.6 ± 3.4 (n = 5), D315C = 31.4 ± 6.0 (n = 5), D315C&I67C = 77.3 ± 12.8 (n = 8). The results show that the expression and the receptor property of the mutants are intact, with no large difference from the WT. As the EC_{50} value of D315C&I67C was higher than that of WT, which is understandable considering the proximity of I67 to the ATP binding site, we used a high concentration of ATP (1 mM) in most of the subsequent experiments.

The observation of a DTT-induced increase in current for the D315C&I67C mutant suggests the formation of a disulfide bridge between the D315C and I67C residues, which disturbs normal gating of the channel. In Fig. 2*F*, Western blotting of the constructs after SDS-PAGE with and without treatment by DTT are shown. Only D315C&I67C showed a dimer formation in the absence of DTT, suggesting that these two residues are forming an inter-subunit Cys–Cys bridge which leads to dimer formation.

Cd^{2+}-induced modification of D315C&I67C in the open state

Our goal was to detect the structural rearrangements of P2X2 associated with ATP- and voltage-dependent gating, by monitoring the change of current amplitude of D315C& I67C by Cys modification. Here we examined modification of D315C&I67C current by the thiol reactive metal Cd^{2+}, in the presence of ATP, using a repeated hyperpolarizing pulse protocol (Fig. 3). Repeated pulse protocols enabled a longer duration of recording at hyperpolarized potentials, avoiding the increase in leak current that occurs when oocytes are voltage clamped at hyperpolarized potentials for a long time. Time lapse changes of normalized maximum inward current amplitudes are shown, in response to application of saturating ATP (1 mM) and subsequent application of 300 μM Cd^{2+} (Fig. 3*A*–*D*). Pretreatment with DTT was not done to avoid complication by residual DTT. In WT and single

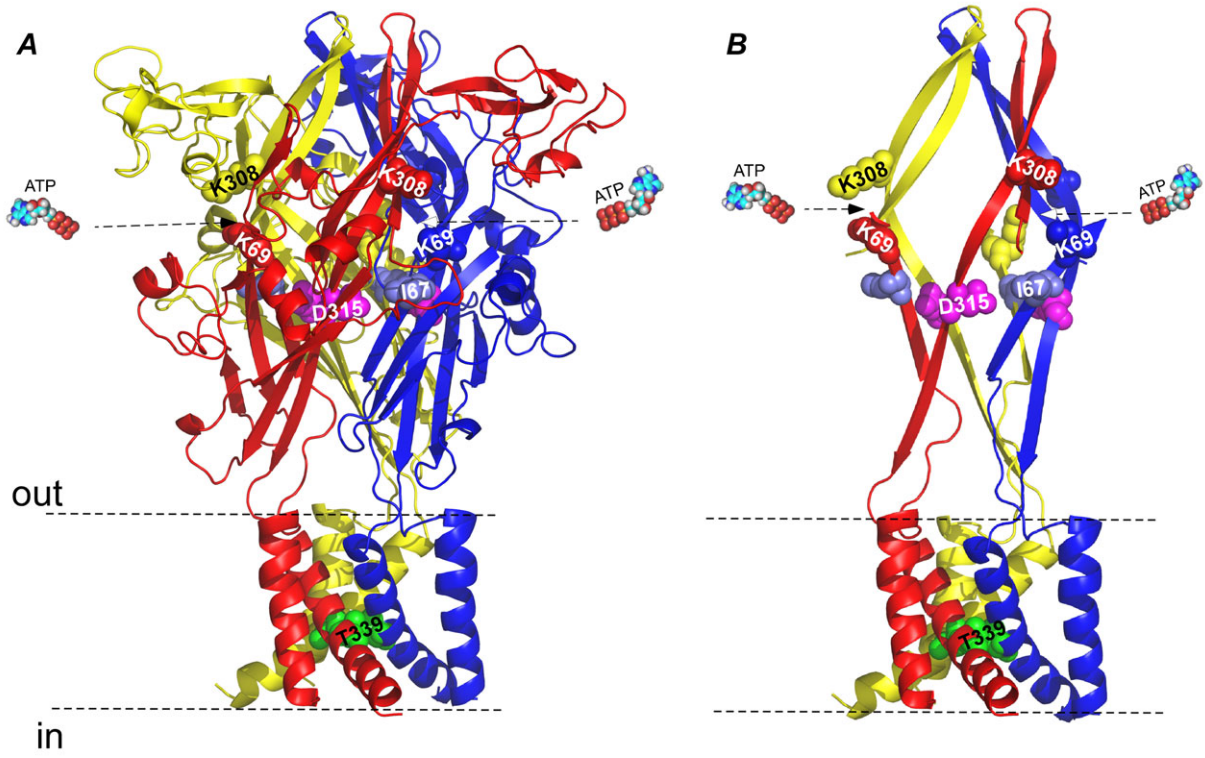

Figure 1. Homology model of the structure of rat P2X2 based on zebra fish P2X4 in the closed state, depicting the location of the ATP binding site, D315 and I67 in the linker region, and T339 in the pore region
A, a side view of the homology model structure of rat P2X2 (Keceli & Kubo, 2009) based on the crystal structure of zebra fish P2X4 in the closed state (Kawate *et al.* 2009). Shown by spheres are: Lys(K)308 and Lys(K)69 in the ATP binding site, Asp(D)315 and Ile(I)67 in the β-sheet linker region, which were mutated to Cys(C) in this study, and Thr(T)339 in the pore region, which was mutated to Ser(S) in this study. *B,* a simplified presentation of *A* to highlight the ATP binding site, transmembrane (TM) region, and the β-sheet structure linking these regions.

mutants (Fig. 3*A*–*C*), a fast increase in the inward current was observed upon ATP application with a slow desensitization, but subsequent application of Cd^{2+} did not induce a prominent further change of the time course of current decline. However, in the case of double mutant D315C&I67C, exposure to Cd^{2+} induced a fast current decline (Fig. 3*D*). In Fig. 3*E*, the cumulative data for the current decline observed after Cd^{2+} application are plotted. Cd^{2+}-induced current decline was significantly higher in the D315C&I67C double mutant than WT and

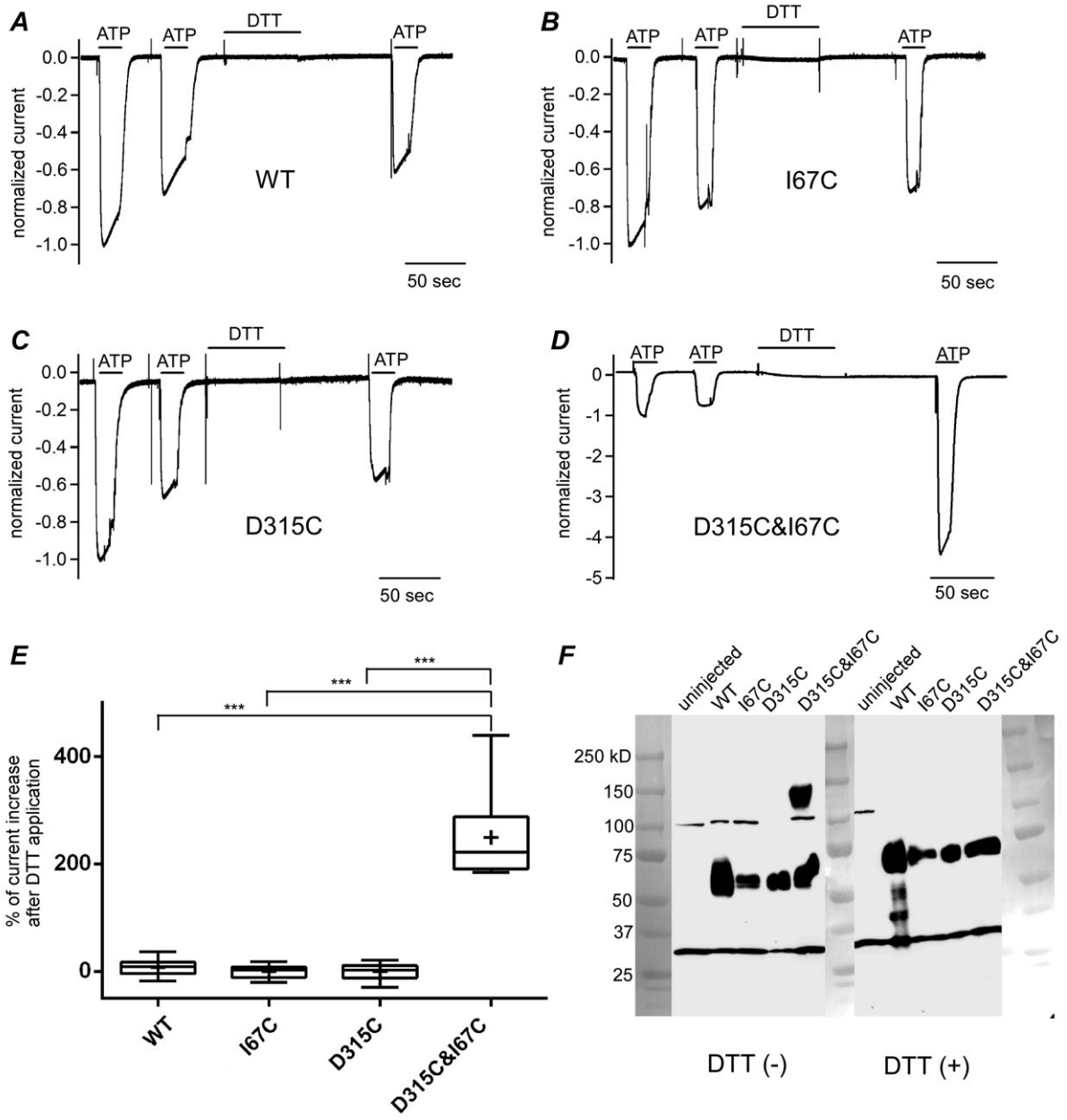

Figure 2. D315C&I67C is a redox-regulated channel
Responses to 1 mM ATP at −80 mV before and after incubation in 10 mM DTT for 1 min with 1 min extensive wash. Shown are responses normalized to the initial response of wild type (WT; *A*), I67C (*B*), D315C (*C*), and D315C&I67C (*D*). *E,* box plots of percentage of current amplitude change by DTT treatment relative to the amplitude of the initial response. Means are shown as plus signs. The bottom and top of each box are the 25th and 75th percentiles, and the line in the middle is the median. Whiskers show the minimum and maximum data values. Data were analysed by one-factor ANOVA and *post hoc* multiple comparisons (***$P < 0.001$, $n = 7$–14). *F,* Western blotting in reducing and non-reducing conditions for WT, I67C, D315C, and D315C&I67C taken in a single image. Photos of size markers taken in the bright field were overlaid.

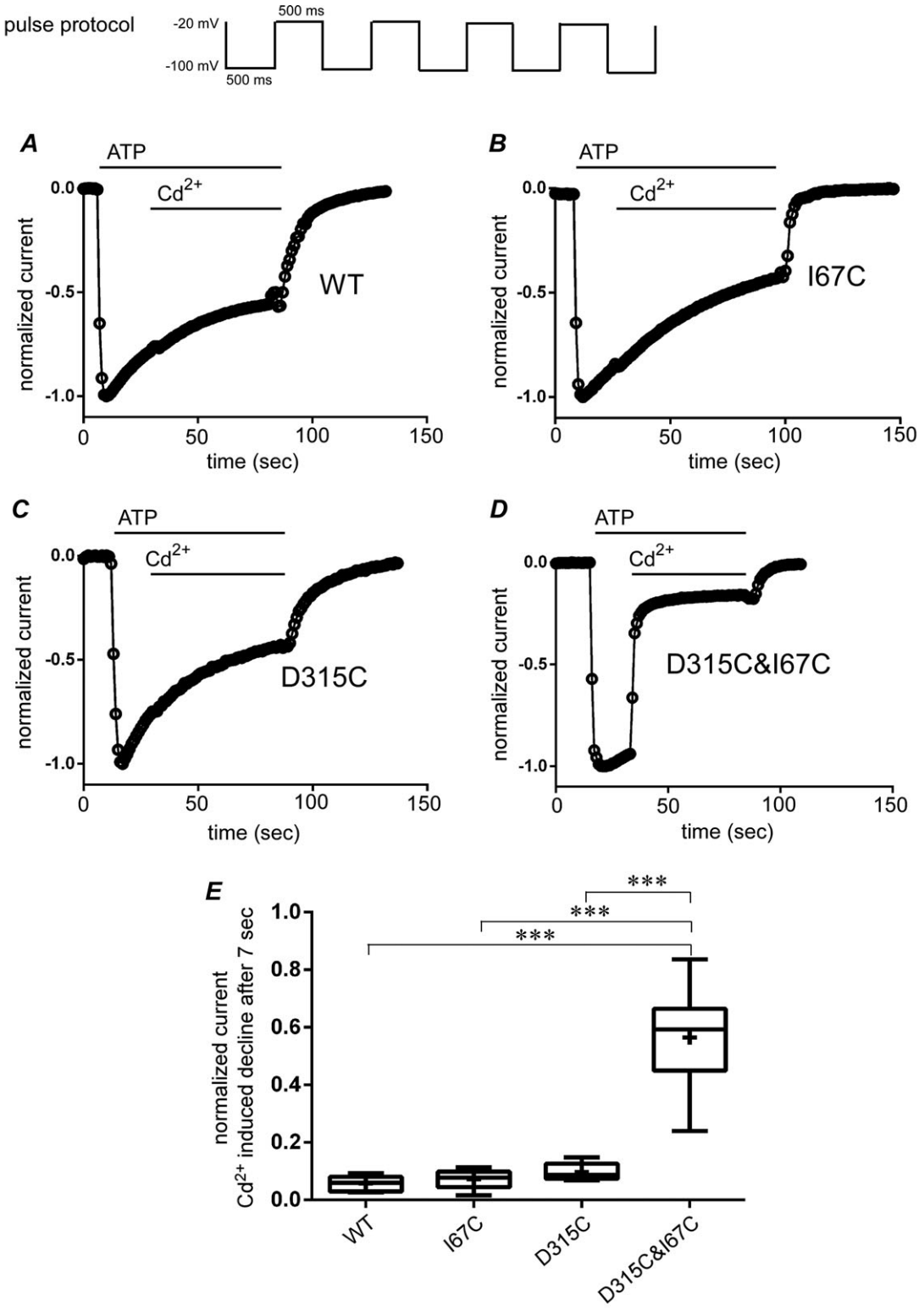

Figure 3. D315C&I67C is modified by Cd^{2+} bridging between D315C and I67C in the presence of ATP
A–D, oocytes were voltage clamped at −20 mV and 500 ms hyperpolarizing pulses to −100 mV were applied repetitively each second as shown at the top. After 1 mM ATP application, 300 μM Cd^{2+} was chase-applied. Time lapse changes of maximum inward currents are shown on a normalized scale for WT (*A*), I67C (*B*), D315C (*C*), and D315C&I67C (*D*). *E,* cumulative data of the fraction of current decline are shown in box plots, as used in Fig. 2*E*. Data were analysed by one-factor ANOVA and *post hoc* multiple comparisons (***$P < 0.001$, $n = 7$–18).

single point mutants ($P < 0.001$, $n = 7$–18) and there were no significant differences among the WT and single mutants.

Upon application of a hyperpolarizing step pulse, voltage-dependent activation can be observed as a gradual increase in the current amplitude. We examined the effect of Cd^{2+} modification on the voltage-dependent activation phase of WT (Fig. 4*A*) and the mutants (Fig. 4*B*–*D*). The hyperpolarization-induced activation phase of D315C&I67C was decelerated after Cd^{2+} application (Fig. 4*D*). Activation time constants (τ, mean ± SEM, in ms) for D315C&I67C before (black arrow) and after (red arrow) Cd^{2+} application were 74 ± 3 and 169 ± 2, respectively, and the difference was statistically significant ($P < 0.001$, $n = 14$). However, no significant differences were observed before and after Cd^{2+} application in WT, I67C and D315C ($n = 12$–20; Fig. 4*E*).

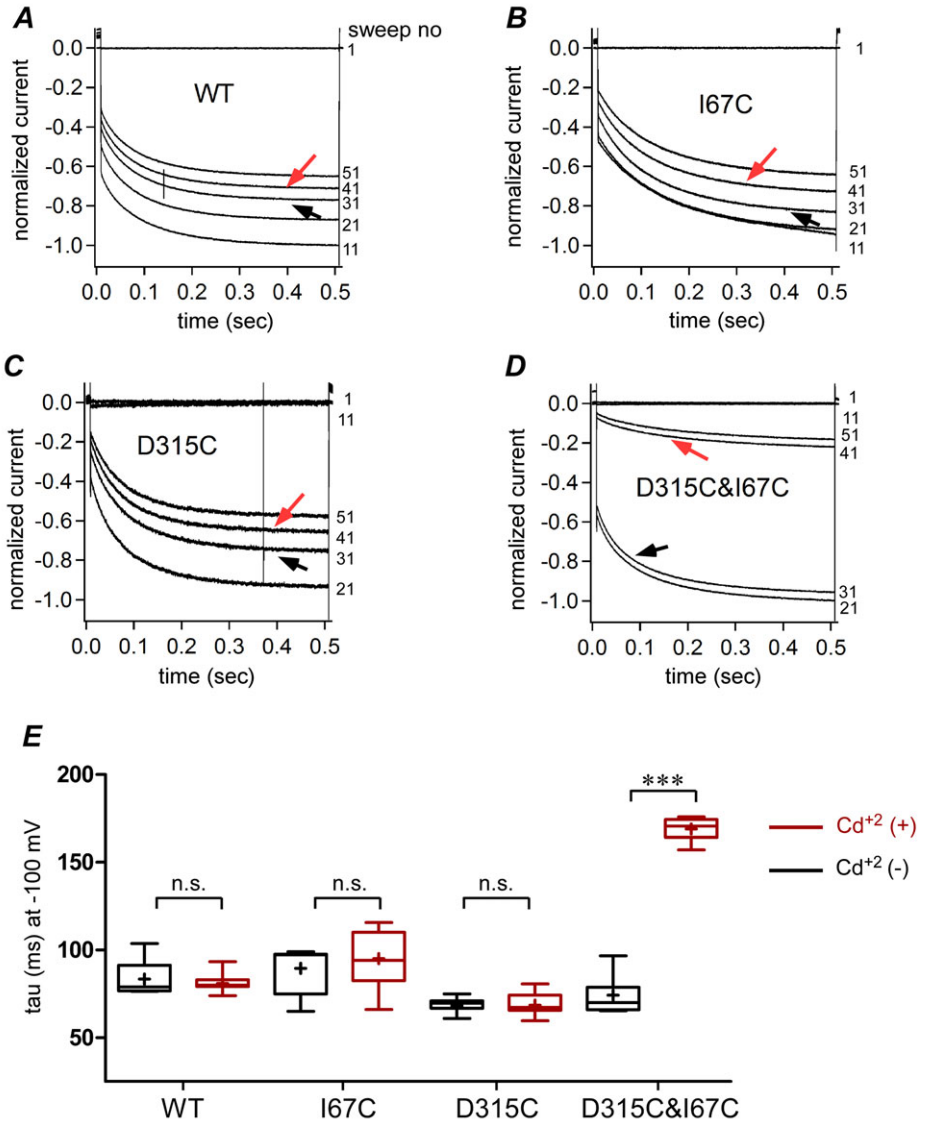

Figure 4. Cd^{2+} decelerates the voltage-dependent gating of D315C&I67C
A–D, representative traces for WT (*A*), I67C (*B*), D315C (*C*), and D315C&I67C (*D*) obtained by the pulse protocol used in Fig. 3. Six traces at 10 s intervals during the first 60 s are shown. 1 mM ATP application activated the channel, and Cd^{2+} was applied at around 30 s for approximately 70 s. Black and red arrows indicate the traces before and after Cd^{2+} application. Note that in D315C&I67C only there is an apparent decline in current amplitude and deceleration of voltage-dependent activation. *E,* voltage-induced activation time constants before and after Cd^{2+} application shown by box plots, as used in Fig. 2*E*. Pairwise comparisons of activation time constants (τ, ms) before and after Cd^{2+} application were performed using Student's *t* test. (***$P < 0.001$, $n = 12$–20).

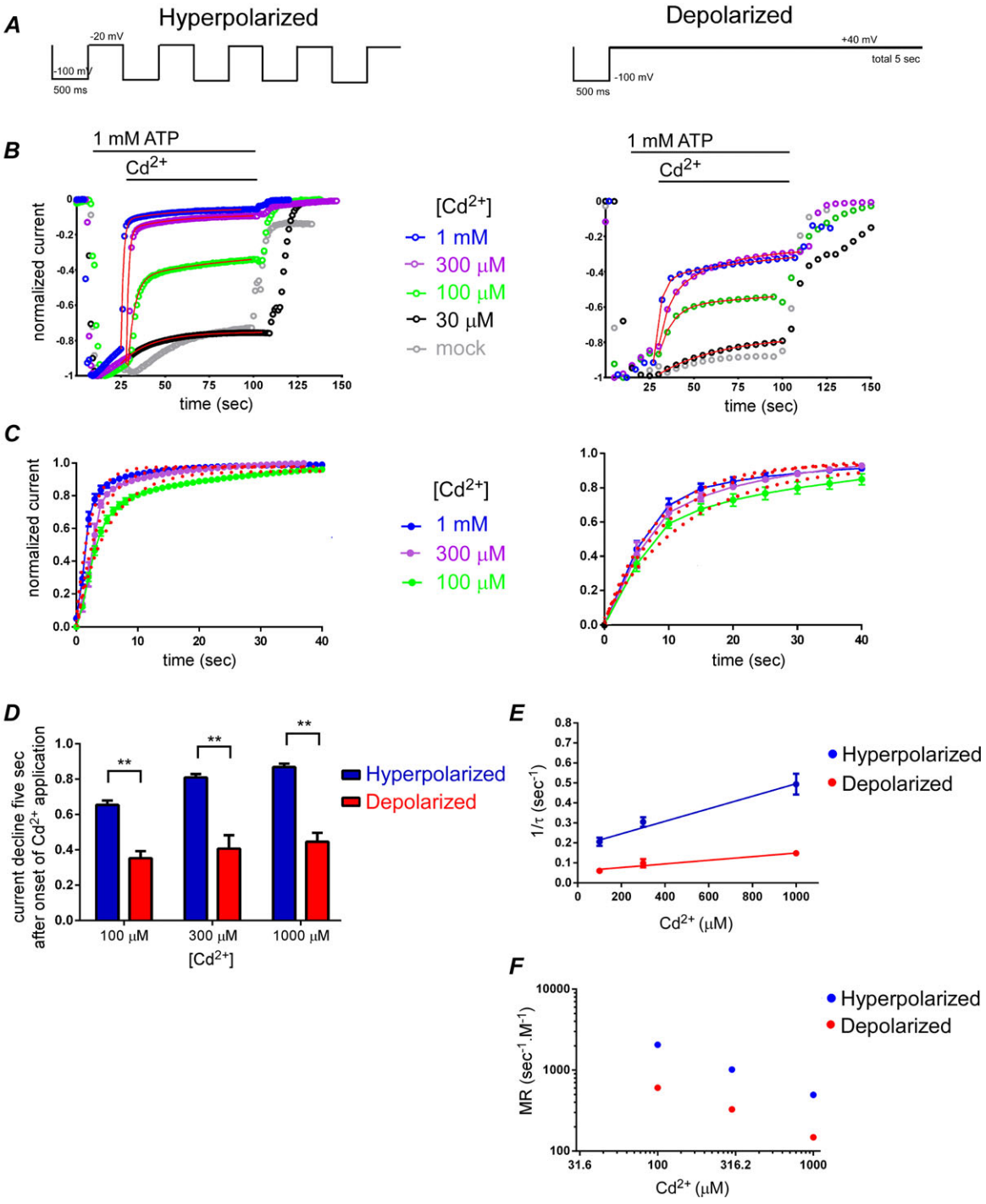

Figure 5. Modification of D315C&I67C by Cd^{2+} in the presence of ATP is voltage dependent
A, pulse protocols used for hyperpolarized (left) and depolarized (right) conditions. *B,* representative traces of time-lapse changes of normalized I_{max} at −100 mV for hyperpolarized (left) and depolarized (right) pulse protocols in response to 1 mM ATP and various [Cd^{2+}]. *C,* data in *B* were normalized by setting the current level at the onset of Cd^{2+} application to be zero, and that at the steady state after approximately 70 s of Cd^{2+} application to be 1.0. The mean and SEM after normalization were calculated (n = 20–26 for hyperpolarized and n = 8–16 for depolarized conditions) and plotted. The mean values were fitted with single exponential functions, shown as red dots. *D,* bar graphs of fraction of current decline at 5 s after the onset of Cd^{2+} application. Data are shown as means ± SEM. Statistical significance was analysed by Student's t test (**$P < 0.01$, n = 8–26). *E,* plots of (1/time constant of current modification (s)) as a function of [Cd^{2+}] in hyperpolarized and depolarized conditions in 1 mM ATP. *F,* plots of modification rate (1/(time constant of current modification × [Cd^{2+}])) as a function of [Cd^{2+}] in 1 mM ATP.

These results show that extracellular application of Cd^{2+} in the presence of ATP modifies D315C&I67C channel activity, presumably via a bridge formation between the two introduced cysteine residues D315C and I67C. It was also shown that Cd^{2+} coordination modifies the voltage-dependent gating property.

Voltage dependence of Cd^{2+}-induced modification of D315C&I67C in the presence of ATP

By comparing the structures of the ATP unbound form (Kawate *et al.* 2009) and the ATP bound form (Hattori & Gouaux, 2012), Hattori & Gouaux proposed that the conformational change of the ATP binding site upon ATP

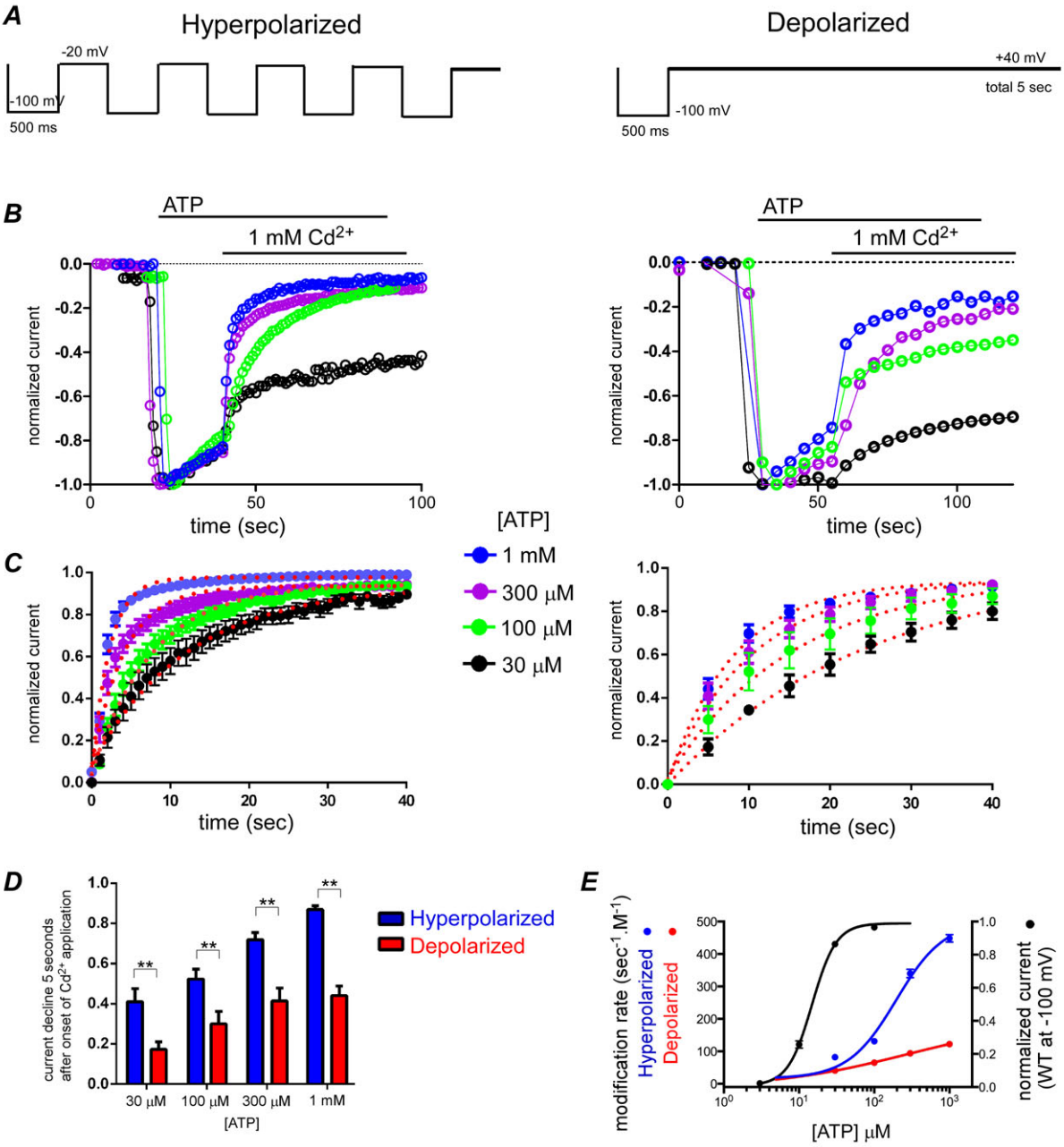

Figure 6. Modification of D315C&I67C by Cd^{2+} is [ATP] dependent
A–D, same as in Fig. 5*A–D*. In *C* and *D*, *n* values were $n = 12–22$ for hyperpolarized and $n = 9–19$ for depolarized conditions. In *D*, Student's *t* test was used for statistical analyses (**$P < 0.01$, $n = 9–22$). *E*, ATP dose–response relationship for WT P2X2 at −100 mV (black) and Cd^{2+} (1 mM) modification rates for D315C&I67C at hyperpolarized (blue) and depolarized (red) conditions as a function of [ATP] are plotted on the same graph. Error bars show SEM. Continuous lines show fits to the Hill–Langmuir equation.

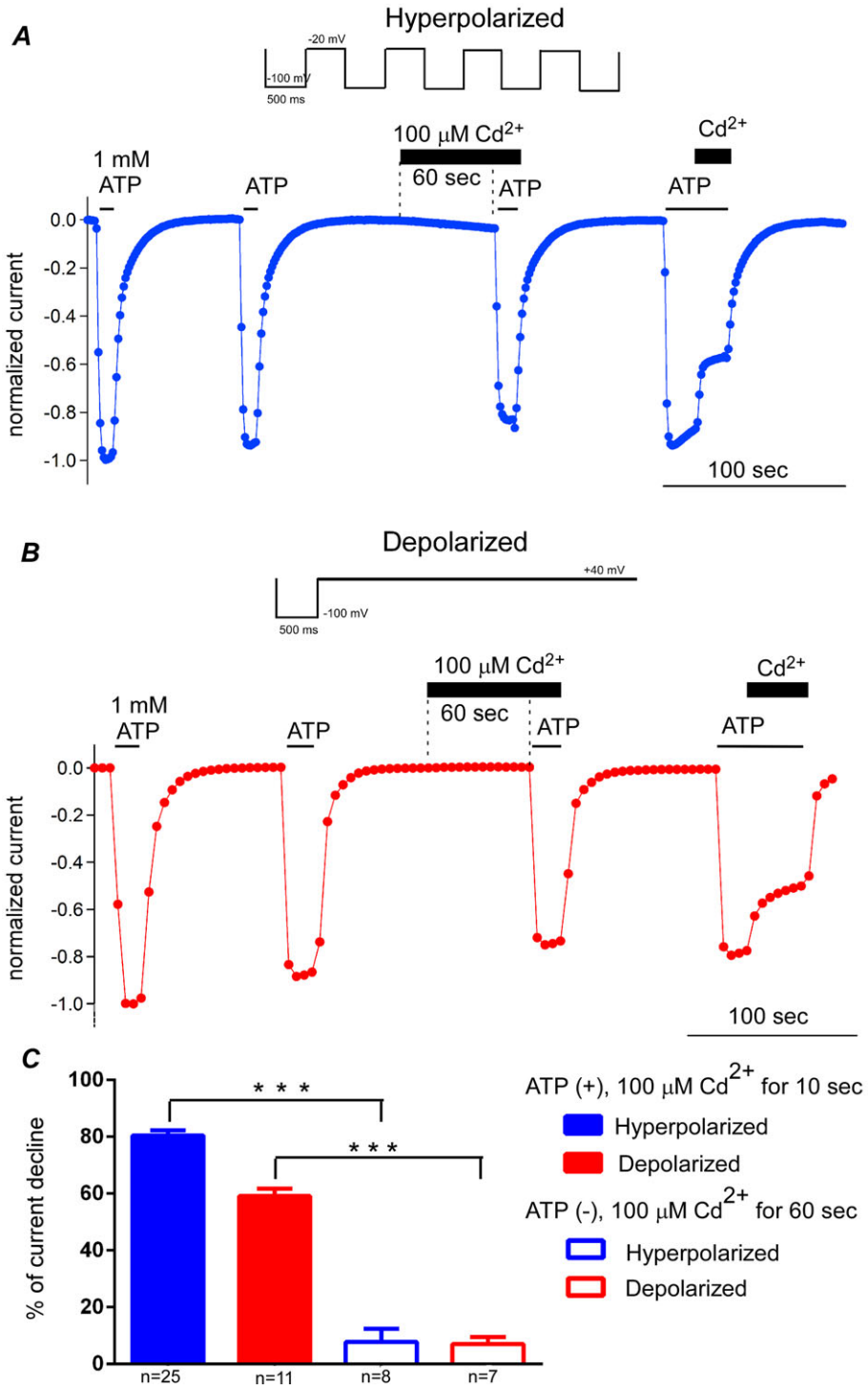

Figure 7. Cd^{2+} modification of D315C&I67C in the absence of ATP
A and *B*, pulse protocols are shown above the representative data for hyperpolarized (*A*) and depolarized (*B*) conditions. Responses to ATP were recorded four times in one set of experiments. The timing of application of 1 mM ATP and 100 μM Cd^{2+} are indicated by bars. The 3rd response was taken after 60 s incubation in Cd^{2+}, and ATP was applied without decreasing [Cd^{2+}]. The decrease in the current amplitude from the 2nd to the 3rd response reflects the Cd^{2+} modification in the absence of ATP. After intensive wash-out of ATP and Cd^{2+}, the 4th response was recorded, and then Cd^{2+} was chase-applied to confirm clear Cd^{2+} modification in the presence of ATP. *C*, the percentage current decline values in 100 μM Cd^{2+} for 10 s in the presence of ATP, taken from the data in Fig. 5 ($n = 25$, 11), and for 60 s in the absence of ATP ($n = 8$, 7) were compared in both hyperpolarized (blue) and depolarized (red) conditions. The differences between the presence and absence of ATP) were analysed by Student's *t* test (***$P < 0.001$).

binding induces deformation and rotation of the linker region and then the transmembrane regions, which subsequently results in the pore opening. Thus, the role of the linker strands in the transmission of the ATP binding signal is obvious from the structural point of view. However, it remains to be elucidated whether or not there are voltage-dependent structural rearrangements in the linker domain.

As the structural rearrangements could be captured as the difference in the extent and the speed of modification by Cd^{2+} between two states, we analysed the Cd^{2+} modification of D315C&I67C in the presence of 1 mM ATP

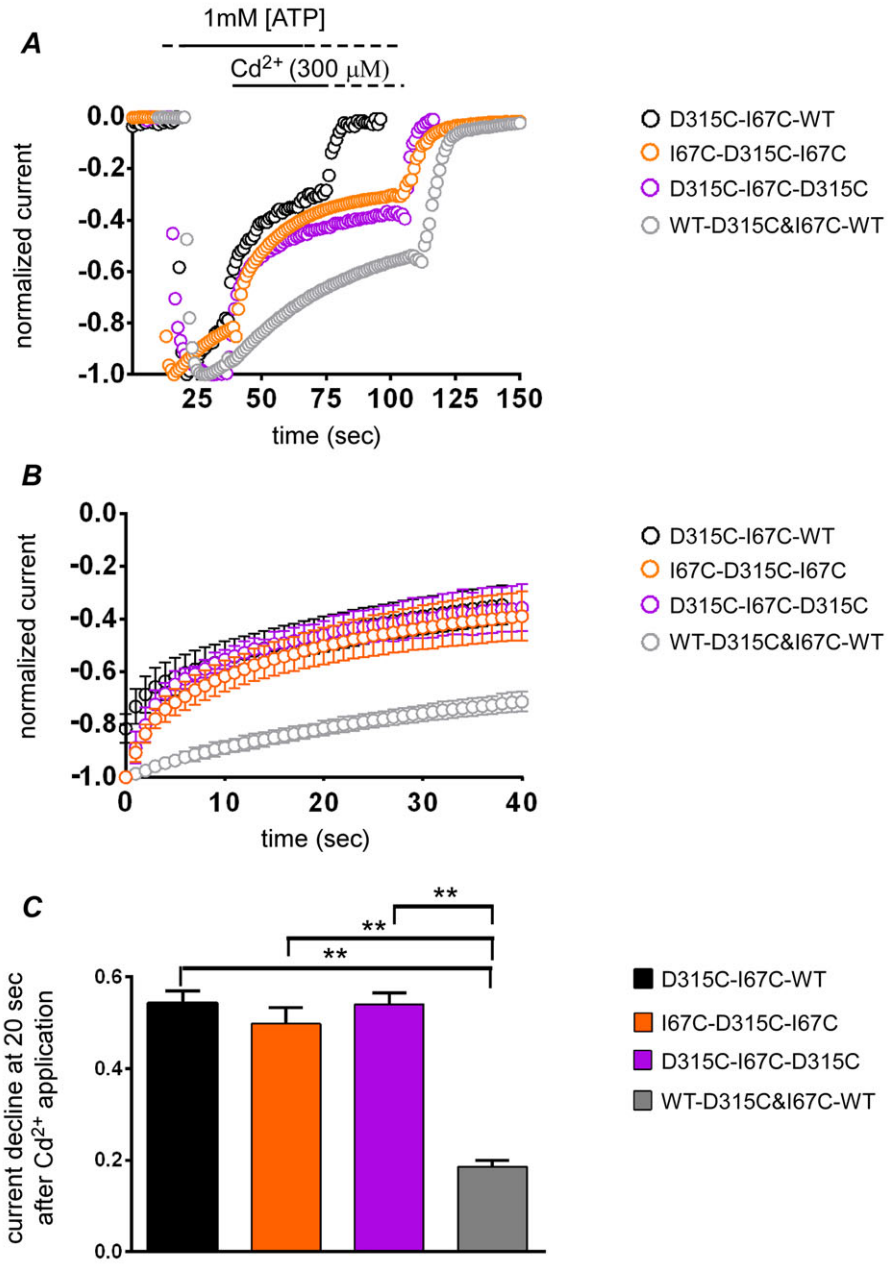

Figure 8. Cd^{2+} bridging between D315C and I67C is inter-subunit
A, representative recordings from the tandem trimer constructs (TTCs) with intra-subunit or inter-subunit Cd^{2+} modification sites. Cd^{2+} modifies TTCs with inter-subunit thiol-modifiable sites, but not the TTC with only an intra-subunit modifiable site (WT-D315C&I67C-WT). *B,* shown are mean and SEM of normalized current from the onset of Cd^{2+} application. *C,* fraction of current decrease after 20 s of Cd^{2+} application (mean ± SEM). One-factor ANOVA and *post hoc* pairwise comparisons showed that the current decline of the TTCs with inter-subunit modifiable site were significantly larger than that with an intra-subunit modifiable site (WT-D315C&I67C-WT; $^{**}P < 0.01$, $n = 7$–12).

using two different pulse protocols. For the hyperpolarized condition, the holding potential was −20 mV and 500 ms hyperpolarizing step pulses to −100 mV were applied once every second (Fig. 5*A*, left). For the depolarized condition, the holding potential was +40 mV and hyperpolarizing step pulses were applied once every 5 s (Fig. 5*A*, right).

Representative traces of the time lapse changes of the inward currents, normalized to the amplitude of the maximum level, are shown in Fig. 5*B*. We observed acceleration of current decline in both conditions with increasing [Cd^{2+}] (Fig. 5*B*). We observed an apparent difference in the rate of Cd^{2+}-induced current decline between hyperpolarized and depolarized conditions. Although an effect of 30 μM Cd^{2+} could be observed, it was hard to discriminate it from the rundown, decay, or desensitization of the channel observed in the absence of Cd^{2+} (Fig. 5*B*). Therefore, we did not include the data for 30 μM Cd^{2+} for further analysis (Fig. 5*C*–*E*).

Data in Fig. 5*B* were further normalized in Fig. 5*C* by setting the current level at the onset of Cd^{2+} application

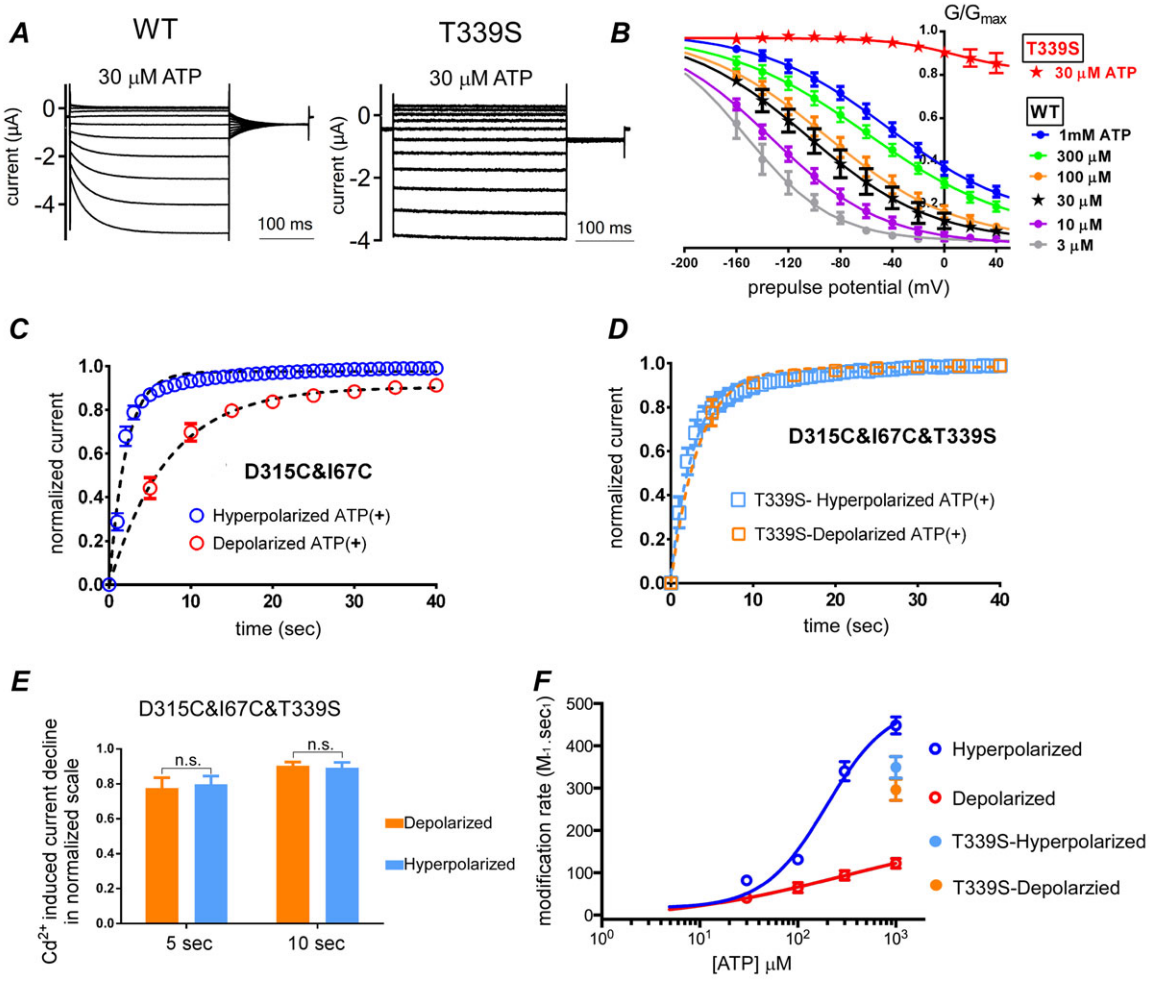

Figure 9. Cd^{2+}-induced modification of D315C&I67C with a voltage-insensitive mutation, T339S
A, voltage- and [ATP]-dependent gating of WT P2X2 (left) and the T339S mutant which lacks voltage-dependent gating (right). Responses were evoked by step pulses from +40 mV to −160 mV in 20 mV decrements from the holding potential of −40 mV in the steady state after application of 30 μM ATP. *B*, mean (± SEM) normalized *G–V* relationship for WT (n = 10) and T339S (n = 5) derived from tail current analysis in various [ATP]. The plots were fitted with the two-state Boltzmann equation. *C* and *D,* normalized Cd^{2+}-induced current decline of D315C&I67C (*C*) and D315C&I67C&T339S (*D*) in depolarized and hyperpolarized conditions, starting from the onset of 1 mM Cd^{2+} application in the presence of 1 mM ATP (mean ± SEM; n = 12–13). Data were fitted with a single exponential function, shown by the dashed black lines. *E,* bar graphs of current decline at 5 s and 10 s after the onset of Cd^{2+} application of D315C&I67C&T339S in depolarized and hyperpolarized conditions. Data are shown as means ± SEM. Statistical analyses were performed by Student's *t* test ($P > 0.05$, n.s.; n = 12–13). *F,* MR by 1 mM Cd^{2+} in 1 mM ATP of D315C&I67C&T339S in hyperpolarized and depolarized conditions are plotted as a function of [ATP], together with the modification rates for D315C&I67C (same as in Fig. 6*E*). Continuous lines show fits to the Hill–Langmuir equation.

to zero, and that at the steady state approximately after 70 s of Cd^{2+} application to 1.0. The mean and SEM after normalization were calculated ($n = 20$–26 in hyperpolarized and $n = 8$–16 in depolarized conditions) and plotted. The mean values were fitted with single exponential functions, and the fits are shown as red dots (Fig. 5*C*). As shown in Fig. 5*D*, the fraction of the current decline 5 s after Cd^{2+} application was significantly different between hyperpolarized and depolarized conditions ($P < 0.01$, $n = 8$–26).

From the fits in Fig. 5*C*, the time constant (τ) of modification was calculated, and $1/\tau$ in various [Cd^{2+}] was plotted (Fig. 5*E*). Then the modification rate (MR), $1/([Cd^{2+}]\,(M) \times \tau\,(s))$, which reflects modification in unit time by unit concentration, was calculated and plotted as a function of [Cd^{2+}] (Fig. 5*F*). In the linear range where

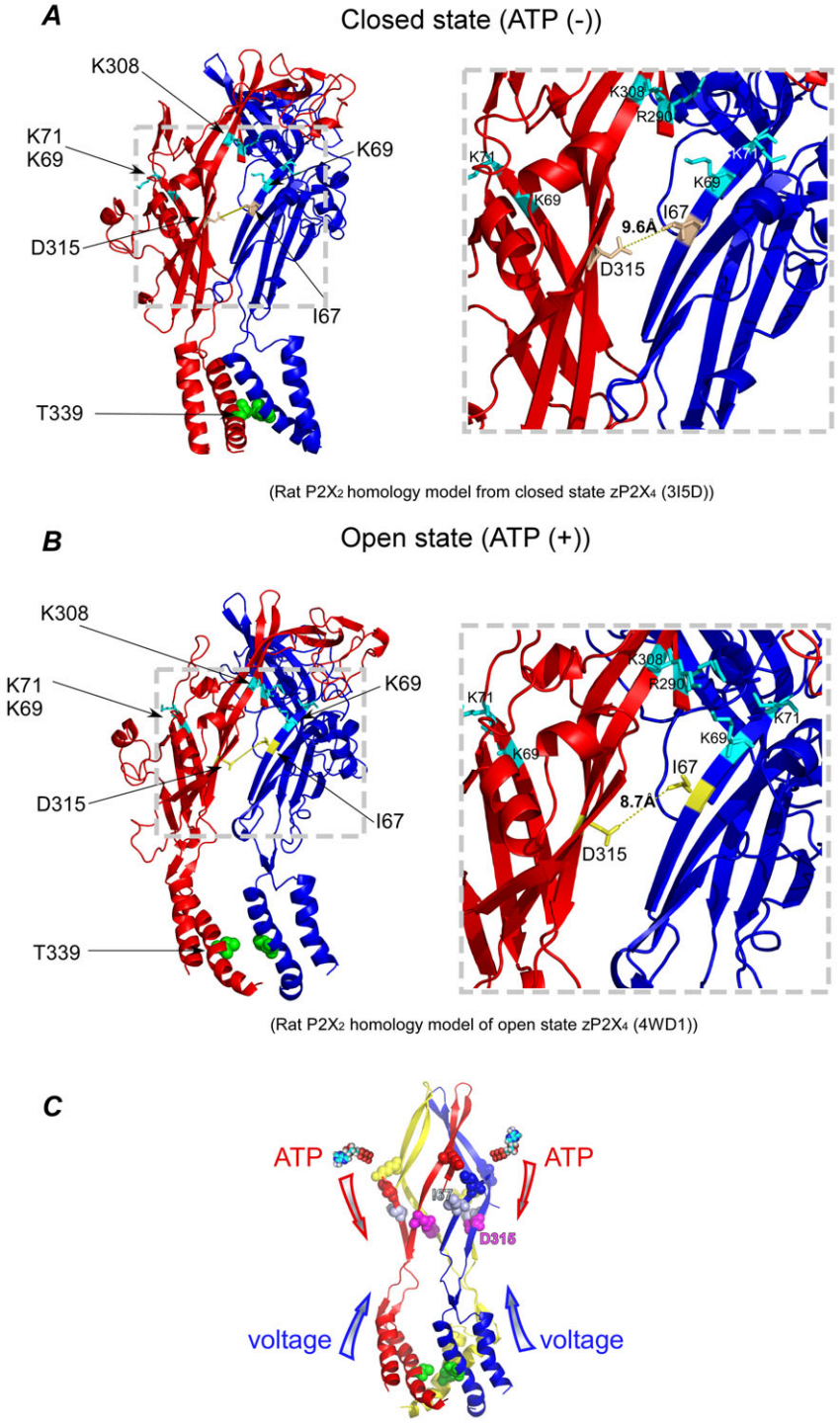

Figure 10. Homology models of the rat P2X2 structure in the closed and open states, highlighting the distance between D315 and I67, and a scheme to show the signal transmission
A and *B*, side views of the homology model based on the crystal structure of zebra fish P2X4 in the closed (*A*) and open state (*B*). Only two subunits are shown in order to clearly depict the inter-subunit Cd^{2+} modification site. The insets show the enlarged views of the β-strands and inter-subunit distances between D315 and I67 in both closed (*A*) and open (*B*) states. Amino acid residues of the adjacent ATP binding site (K69 andK71 on the blue subunit and R290 and K308 on the red subunit) are depicted in light blue. *C*, a schematic drawing of P2X2 in open state, illustrating the convergence of transmission of two signals at the β-strand linker region, a ligand-induced signal from the ATP binding site and the voltage-induced signal from the TM helices.

the effect increased proportionally with increasing Cd^{2+} concentration, MR is expected to be constant. From the data in Fig. 5*F*, it is clear that 1 mM Cd^{2+} is above the linear range. Another possible explanation for non-constant MR is that in low Cd^{2+} there is contamination of endogenous decay which made the evaluated MR larger. In all examined Cd^{2+} concentrations, MR in the hyperpolarized condition was significantly larger than that in the depolarized condition ($P < 0.01$, $n = 8$–26). Taken together, the results clearly demonstrate that Cd^{2+} modification is voltage dependent.

ATP concentration dependence of Cd^{2+}-induced modification

To examine the ATP concentration dependence of Cd^{2+} modification, we performed similar experiments to Fig. 5 in the presence of a constant Cd^{2+} concentration (1 mM) and various [ATP] (Fig. 6*A*). Cd^{2+}-induced modification was accelerated with increasing [ATP] and was again faster in the hyperpolarized than in the depolarized condition (Fig. 6*B*–*D*). As the Cd^{2+}-induced current decline was not clearly observed or almost negligible in 10 μM and lower concentrations of ATP, the data were not included in the analyses. As shown in Fig. 6*D*, the difference in modification after 5 s of Cd^{2+} application was statistically significant ($P < 0.01$, $n = 9$–26).

The calculated MR values from the fitting of the data in Fig. 6*C* are plotted in Fig. 6*E*. It is clear that MR increases with increasing [ATP] and is also higher in the hyperpolarized than in the depolarized condition. We also observed an apparent rightward shift of [ATP] *vs.* MR relative to the ATP dose–response relationship of WT P2X2 at −100 mV (Fig. 6*E*). This might be because a higher occupancy probability of the ATP binding site by ATP might be needed for Cd^{2+} modification than for current activation. In summary, the ATP concentration dependence suggests that the modification by Cd^{2+} is more prominent in the open or ATP bound state than in the closed or ATP unbound state.

The results also show that the effect of Cd^{2+} is not due to chelation of ATP by Cd^{2+}, because, if this were the case, the modification would be expected to be more prominent in lower ATP, which is opposite to the observed result.

Cd^{2+}-induced modification in the absence of ATP

To further investigate the difference in the Cd^{2+} modification in the open state *vs.* closed state, it would be ideal to analyse Cd^{2+} modification in the ATP-free condition. The problem is that the current cannot be monitored in the absence of ATP. To monitor the Cd^{2+} effect in the absence of ATP, we first performed an experiment to compare two ATP responses without Cd^{2+}, before and after incubation with Cd^{2+} and no ATP. No significant current decline was observed (data not shown). However, even in experiments such as that shown in Fig. 3, in which the current clearly declined in Cd^{2+}, we observed that the current amplitude evoked by the 2nd ATP application after washout of Cd^{2+} was close to the initial level (data not shown). These results suggest that Cd^{2+} modification of D315C&I67C is not irreversible and can be washed out. Thus, the apparent lack of Cd^{2+} modification in the absence of ATP in the above experiment might be due to wash out of Cd^{2+}, and we could not draw a conclusion about Cd^{2+} modification in the ATP-free condition.

We instead performed the experiment shown in Fig. 7*A* (hyperpolarized) and *B* (depolarized). We applied 1 mM ATP twice to confirm stable responses, washed out ATP, applied 100 μM Cd^{2+} for 60 s, and then applied 1 mM ATP while maintaining the Cd^{2+} concentration to record the 3rd response. This 3rd response was expected to reflect modification by Cd^{2+} for 60 s in the absence of ATP. We compared the peak current amplitudes of the 2nd and the 3rd responses, and calculated the fraction of decline. The decline would be somewhat overestimated, because it could include the effect of Cd^{2+} modification in ATP for a few seconds at the beginning of the 3rd response. The reason for using 100 μM Cd^{2+} here, instead of 1 mM, was to minimize this modification in the co-presence of ATP and Cd^{2+}. After extensive wash out of ATP and Cd^{2+}, we applied ATP again to obtain the 4th response, after which we chase-applied Cd^{2+} to confirm the clear Cd^{2+} modification in the presence of ATP.

In Fig. 7*C*, the fraction of current decline at 10 s after application of 100 μM Cd^{2+} in the presence of 1 mM ATP (filled bars) and after 60 s incubation in 100 μM Cd^{2+} in the absence of ATP (open bars) was compared in hyperpolarized and depolarized conditions. In spite of the 6 times longer incubation time in Cd^{2+} in the ATP-free condition than in ATP, the extent of current decline was approximately 10 times less. The data values in ATP were taken from the experiment in Fig. 5, not from the 4th response in Fig. 7 with chase application of Cd^{2+}, because the 4th response was recorded after applying Cd^{2+} twice and the effect of the 1st Cd^{2+} application might have remained. Although comparison of MR was not possible, the Cd^{2+} modification was significantly smaller in the absence than in the presence of ATP ($P < 0.01$, $n = 7$–25).

Cd^{2+} bridging of D315C&I67C is not intra- but inter-subunit

To determine whether the Cd^{2+}-induced modification is inter-subunit or intra-subunit, we performed similar modification analyses on TTCs harbouring D315C and I67C mutations in various combinations. While there was no apparent Cd^{2+}-induced current decline

in WT-D315C&I67C-WT, where the modifiable site is intra-subunit, all other combinations that allow one inter-subunit modifiable site showed instantaneous current decline immediately after Cd^{2+} application (Fig. 8*A*–*C*). The difference in modification at 20 s was statistically significant ($P < 0.01$, $n = 7$–12; Fig. 8*C*). Cd^{2+}-induced current decline was also accompanied by an apparent deceleration of the voltage-induced activation upon hyperpolarization (data not shown), as observed in Fig. 4*D*. The results clearly show that only one inter-subunit Cd^{2+} bridge formation in the trimer is sufficient to induce current decrease.

Cd^{2+}-induced modification of D315C&I67C with the T339S pore mutation

Cd^{2+} modification experiments in Fig. 5 revealed that P2X2 shows voltage-induced conformational changes at the linker domain. As this localization is outside the electrical field of the membrane (Fig. 1) it is very unlikely that the Cd^{2+} effect at this site is under the direct influence of membrane potential. We aimed to clarify whether voltage-induced rearrangements of the linker domains are coupled with those of the transmembrane helices, which are in the electrical field of the membrane. Therefore, we used a pore mutant, T339S, which abolishes the voltage-dependent gating at a relatively high concentration of ATP (Keceli & Kubo, 2009; Fig. 9*A* and *B*).

As reported previously (Fujiwara *et al.* 2009; Keceli & Kubo, 2009), in the steady state after application of ATP, the P2X2 receptor shows a single exponential voltage-induced activation phase upon hyperpolarization (Fig. 9*A*), and tail current analysis reveals an [ATP]-dependent shift of the *G*–*V* curve to depolarized potentials (Fig. 9*B*). In contrast, the T339S pore mutant shows only minimal voltage-dependent activation in high [ATP] (Fig. 9*A* and *B*; Keceli & Kubo, 2009). Tail current analysis revealed that the channel was almost equally active at all membrane potentials (Fig. 9*B*), showing a lack of voltage-dependent gating. Macroscopic recordings from the T339S mutant do not show activity in the absence of ATP (Keceli & Kubo, 2009).

We recorded and analysed the modification by Cd^{2+} of D315C&I67C&T339S in both depolarized and hyperpolarized conditions, and compared it with that of D315C&I67C. Current changes after 1 mM Cd^{2+} application in 1 mM ATP are shown for D315C&I67C ($n = 25$–26; Fig. 9*C*) and D315C&I67C&T339S ($n = 12$–13; Fig. 9*D*). We observed that the rate of current decline for D315C&I67C&T339S was highly similar at depolarized and hyperpolarized potentials (Fig. 9*D*). Cd^{2+}-induced current decline at depolarized and hyperpolarized potentials did not show a statistical difference at 5 or 10 s after the onset of Cd^{2+} application (for both conditions $P > 0.05$, $n = 12$–13; Fig. 9*E*). Calculated MR values for the T339S mutant were also similar in depolarized and hyperpolarized conditions, and the difference was not statistically different (Fig. 9*F*). The results suggest that linker domains, which play a role in the ATP binding signal transmission to the pore, are also coupled to TM helices in a voltage-dependent manner.

Discussion

Conformational state transitions from closed to open occur in ion channels in response to voltage and/or binding of a ligand. Voltage-dependent gating is primarily attributed to conformational changes of a voltage sensor, a cluster of charged amino acid residues in the transmembrane (TM) helices, which induces rearrangement of the channel pore from closed to open. However, there are membrane proteins that show voltage sensitivity even though they do not have a canonical voltage sensor domain, such as the nicotinic acetylcholine receptor (Charnet *et al.* 1992; Figl *et al.* 1996), the muscarinic ACh receptor (Ben-Chaim *et al.* 2003, 2006) and the metabotropic glutamate receptor (Ohana *et al.* 2006). The detailed mechanism of non-canonical voltage sensing is not yet fully known.

We previously showed that the extracellular ATP gated cation channel P2X2 has intrinsic voltage sensitivity in spite of the absence of a canonical voltage sensor (Fujiwara *et al.* 2009; Keceli & Kubo, 2009). Although a voltage-dependent gating property of P2X2 has been identified and shown to be an intrinsic property of the molecule (Fujiwara *et al.* 2009), the structural background of this property remains to be solved. It is of interest to reveal how voltage-induced structural rearrangements take place and spread in the molecule and how the ligand- and voltage-dependent rearrangements are integrated.

In this study, we aimed at characterization of the voltage- and ligand-dependent structural rearrangements at the linker domain located between the ATP binding sites and TM helices. State-dependent conformational rearrangements associated with gating can be revealed by introduction of cysteine residues by mutagenesis and comparison of the rate and extent of chemical modification by thiol-modifying reagents in different states. Chemical bond formations can be monitored electrophysiologically only when they change the current amplitude. We successfully identified a suitable pair of residues that formed a Cd^{2+}-modifiable site when mutated to cysteine (D315 and I67 located at β-14 and β-1 in the linker region; Fig. 1*B*), and analysed the state-dependent conformational changes at this position.

D315C&I67C is a redox-augmented channel

We observed initially that after application of the reducing reagent DTT, D315C&I67C showed a remarkable increase

in current amplitude. This effect was not observed in WT or single point mutants, showing the presence of native disulfide bridge formation between the introduced Cys residues that counteracts the activation of the channel (Fig. 2*D*). Western blotting analysis also revealed that D315C&I67C formed dimers in addition to monomers (Fig. 2*F*), showing the presence of inter-subunit Cys–Cys bridge formation. The lack of a trimer band and presence of the monomer might be due to the scarcity of the bonds, because of low bonding probability and/or inhibition of the second bond by the structural change induced by the first bond. In agreement with the presence of monomer, we recorded functional current before the application of DTT.

From the snapshots based on the homology modelling of the crystal structure (Fig. 10), the distance between the two residues is too large for the formation of a Cys–Cys bridge (2.1 Å) in both the closed and open states. However, the extracellular domains of the molecule in Fig. 10 are shown to undergo reorientation, i.e. a bending and separation of β-strands, upon the transition from the closed to the open state (Kawate *et al.* 2009; Hattori & Gouaux, 2012). This suggests a considerable structural rearrangement of the linker strands in transmitting the ATP binding signal to the TM helices. The native Cys–Cys bridge formation between the D315C and I67C residues might be due to considerable flexibility of this site. Roberts *et al.* using MTSEA-biotinylation and mapping the ATP sensitive accessibility of introduced cysteine residues in extracellular domains of the molecule, showed evidence for significant structural rearrangements of the extracellular domains in the human $P2X_1$ receptor upon ATP activation (Roberts *et al.* 2012). Stelmashenko *et al.* by introducing pairs of cysteine residues simultaneously in extracellular β-strands, observed a significant reduction in channel activation prior to the application of the reducing reagent (Stelmashenko *et al.* 2012).

Another possible explanation for native Cys–Cys bridge formation in our construct is that the large inter-subunit crevices in the open state of the crystal structure (Hattori & Gouaux, 2012) might actually be missing in P2X2 embedded in the lipid membrane, as reported by Heymann *et al.* based on a molecular dynamics simulation (Heymann *et al.* 2013). Proximity of subunits might enable Cys–Cys bridge formation between substituted Cys residues in the open state.

Conformational changes revealed by analysis of the state dependence of Cd^{2+}-induced modification of D315C&I67C

Although previous studies have shown structural rearrangements of the extracellular domains upon ATP binding, no study until now has been conducted to elucidate the voltage dependence of these structural rearrangements.

When Cd^{2+} was applied in the open state in the presence of ATP, an instantaneous decline in current amplitude was observed, suggesting a –S–Cd–S– bridge formation between the D315C and I67C residues, as this effect was observed neither in WT nor in the single mutants (Fig. 3). Moreover, we observed that Cd^{2+} application decelerated the voltage-dependent activation upon hyperpolarization in D315C&I67C (Fig. 4), showing an influence of Cd^{2+} bond formation in the linker region on the voltage-dependent gating.

Next, we compared the effect of Cd^{2+} in the presence of ATP in hyperpolarized and depolarized conditions to examine the existence of any voltage-dependent structural rearrangement in the linker domains besides that induced by ligand binding. We observed an apparent difference in the rate of current decline after application of Cd^{2+} between hyperpolarized and depolarized conditions (Fig. 5). The fraction of declined current and the MR in various [Cd^{2+}] (Fig. 5*D* and *F*) and in various [ATP] (Fig. 6*D* and *E*) showed a clear and significant difference between hyperpolarized and depolarized conditions. Our results demonstrate that there is a voltage-dependent structural rearrangement in the presence of ATP in the linker region, at a considerable distance from the electrical field of the membrane.

As we simply analysed the current decline kinetics without subtracting the native current decay and/or desensitization in the absence of Cd^{2+}, the MR, especially in low Cd^{2+} is overestimated. This could explain higher MR values in low Cd^{2+} (Fig. 5*F*). Also, the relatively low MR in high Cd^{2+} could be due to saturation of the effect.

We also compared the [ATP]–MR plot with the ATP dose–response relationship at −100 mV, as we used −100 mV for the repetitive hyperpolarizing pulses (Fig. 6*E*). We observed an apparent rightward shift of the MR plot relative to the ATP dose–response relationship. Possible reasons are that a higher ATP binding probability is necessary for Cd^{2+} modification to occur, or that three bound ATP molecules are necessary for Cd^{2+} modification, in contrast to current activation which is triggered by two bound ATP molecules (Keceli & Kubo, 2014).

Modification by Cd^{2+} in the ATP-free (closed) state was also analysed (Fig. 7). Prolonged treatment (60 s) with 100 μM Cd^{2+} had a very limited inhibitory effect on the current. This effect was approximately 10 times smaller than the effect of 100 μM Cd^{2+} applied for 10 s in the presence of ATP. These results clearly demonstrate that there is a conformational change of the linker region in the transition between ATP-free (closed) and ATP-bound (open) states. As the effect in the absence of ATP was almost negligible, we could not detect a voltage-dependent

change of Cd^{2+} modification in the ATP-free (closed) state (Fig. 7*C*).

The spontaneous dimer formation of the D315C&I67C mutant in the absence of reducing reagent shown by Western blot (Fig. 2*F*), and the absence of Cd^{2+} modification for the TTCs which harbour a single intra-subunit thiol-modifiable site (Fig. 8) confirm that Cd^{2+} modification takes place not in an intra- but in an inter-subunit manner. The TTC experiments also showed that Cd^{2+} can modify channel gating, even if it forms only one inter-subunit bridge, by affecting the rearrangements of two adjacent subunits (Fig. 8). This is consistent with our previous data showing that two subunits need to be functionally intact for the normal transmission of the ATP binding signal to the gating of P2X2 (Keceli & Kubo, 2014). While one inter-subunit Cd^{2+} modification can result in an apparent decline in channel activity, the rate of the current decline was slower than with three inter-subunit Cd^{2+} modifications. This could be due to the lower probability of Cd^{2+} bond formation in the case of one modification site than in that of three sites (Fig. 5*B* and Fig. 8).

Structural background of the inter-subunit bridging of D315C and I67C by Cd^{2+} in the open state

Cd^{2+} has been used as a Cys reactive reagent in many structure–function studies (Yellen *et al.* 1994; Contreras *et al.* 2008; Raghuraman *et al.* 2012), including studies of P2X2 receptors (Li *et al.* 2008, 2010; Heymann *et al.* 2013). Cd^{2+} binding sites in proteins usually involve multiple coordinating side chains and are likely to be either in an octahedral or tetrahedral geometry. The distance needed to form a Cd^{2+} bridge between two Cys residues is ∼5 Å (Narula *et al.* 1995; Naylor *et al.* 1998; Raghuraman *et al.* 2012). It has been reported that Cd^{2+} forms a bond with one Cys at approximately ∼2.70 Å distance (Rulisek & Vondrasek, 1998). As there is no His or Cys in close proximity to D315 and I67, Cd^{2+} is more likely to be in a tetrahedral conformation with two H_2O molecules rather than being in an octahedral geometry.

We analysed the structural correlates of the Cd^{2+} localization on our homology model of rat P2X2 based on the crystal structure of zebra fish P2X4 in the closed (Kawate *et al.* 2009) and in the open state (Hattori & Gouaux, 2012) (Fig. 10*B*). To show the proximity of D315 and I67 to the ATP binding site, critical amino acid residues for ATP binding (K69 and K71 on the blue subunit and R290 and K308 on the red subunit) are highlighted in light blue. Considering the side chain localizations of D315C and I67C, which are facing each other from adjacent subunits, Cd^{2+} is highly likely to be located inbetween the two inter-subunit Cys residues (Fig. 10*B*). The measured distance between D315 and I67 from two adjacent subunits in the open state is around ∼8.7 Å (Fig. 10*B*), which is ∼3 Å larger than the distance for a Cd^{2+} bridge (Narula *et al.* 1995; Naylor *et al.* 1998; Raghuraman *et al.* 2012). Heymann *et al.* recently proposed a structure for membrane-embedded P2X2 in the open state, based on their molecular dynamics simulation and intensive structure–function analyses (Heymann *et al.* 2013). They proposed that relative to the open state X-ray structure, the TM helices are translocated 1.3 Å towards the central axis, the twist of the TM2 three-helix bundle is increased by 10 deg, and each TM2 helix is rotated 5 deg counterclockwise around its helical axis (Heymann *et al.* 2013). The shift of TM helices towards the central axis suggests that the linker strands would shift in the same manner and inter-subunit distances would become ∼2.6 Å closer. Our experimental data for Cd^{2+} effects support this new open state structure model. As there is no structural information at all as to voltage dependence, the structural background of the voltage-dependent change of the Cd^{2+} modification remains unknown.

Implications of voltage-dependent Cd^{2+} modification at the extracellular linker region

Voltage-dependent differences in the Cd^{2+}-induced modification of the linker region revealed voltage-dependent structural rearrangements at this site. The Cd^{2+} binding site, which appears to be ∼30 Å distant from the TM helices in the structural model of P2X2, is outside the electrical field of the membrane (Figs 1, 10). Therefore, it is all the more interesting to elucidate the origin of the voltage-dependent structural rearrangements at the Cd^{2+} binding site. We hypothesized that the voltage-dependent structural rearrangements of the linker domains arise as a consequence of the spread of rearrangements in the TM domains. In order to examine this possibility, we analysed the MR by Cd^{2+} of T339S, a pore mutant that abolishes the voltage-dependent gating (Keceli & Kubo, 2009). The Cd^{2+} modification rate of D315C& I67C with the T339S mutation showed no clear voltage dependence (Fig. 8*C* and *D*). Our results demonstrate that the role of the linker strands is not limited to the transmission of the ATP binding-induced signal shown by the structural data, and that the information of membrane voltage change is transmitted from the TM to the linker region. Although voltage-induced structural rearrangements are expected to be confined to a region in close proximity to the electrical field of the membrane, i.e. TM helices, our overall results suggest that membrane potential changes actually induce conformational changes throughout the P2X2 molecule, even in the distant extracellular linker domains. It is possible that extended voltage-induced conformational changes might even influence the

ligand-binding event. The data we obtained in this study will give an insight into the voltage-dependence of gating and other events in ion channels and receptors without a canonical voltage sensor.

References

Arnold K, Bordoli L, Kopp J & Schwede T (2006). The SWISS-MODEL workspace: a web-based environment for protein structure homology modelling. *Bioinformatics* **22**, 195–201.

Ben-Chaim Y, Chanda B, Dascal N, Bezanilla F, Parnas I & Parnas H (2006). Movement of 'gating charge' is coupled to ligand binding in a G-protein-coupled receptor. *Nature* **444**, 106–109.

Ben-Chaim Y, Tour O, Dascal N, Parnas I & Parnas H (2003). The M2 muscarinic G-protein-coupled receptor is voltage-sensitive. *J Biol Chem* **278**, 22482–22491.

Bordoli L, Kiefer F, Arnold K, Benkert P, Battey J & Schwede T (2009). Protein structure homology modeling using SWISS-MODEL workspace. *Nat Protoc* **4**, 1–13.

Brake AJ, Wagenbach MJ & Julius D (1994). New structural motif for ligand-gated ion channels defined by an ionotropic ATP receptor. *Nature* **371**, 519–523.

Charnet P, Labarca C, Cohen BN, Davidson N, Lester HA & Pilar G (1992). Pharmacological and kinetic properties of $\alpha 4\beta 2$ neuronal nicotinic acetylcholine receptors expressed in *Xenopus* oocytes. *J Physiol* **450**, 375–394.

Contreras JE, Srikumar D & Holmgren M (2008). Gating at the selectivity filter in cyclic nucleotide-gated channels. *Proc Natl Acad Sci U S A* **105**, 3310–3314.

Figl A, Labarca C, Davidson N, Lester HA & Cohen BN (1996). Voltage-jump relaxation kinetics for wild-type and chimeric β-subunits of neuronal nicotinic receptors. *J Gen Physiol* **107**, 369–379.

Fujiwara Y, Keceli B, Nakajo K & Kubo Y (2009). Voltage- and [ATP]-dependent gating of the P2X2 ATP receptor channel. *J Gen Physiol* **133**, 93–109.

Fujiwara Y & Kubo Y (2004). Density-dependent changes of the pore properties of the P2X2 receptor channel. *J Physiol* **558**, 31–43.

Hattori M & Gouaux E (2012). Molecular mechanism of ATP binding and ion channel activation in P2X receptors. *Nature* **485**, 207–212.

Heymann G, Dai J, Li M, Silberberg SD, Zhou HX & Swartz KJ (2013). Inter- and intrasubunit interactions between transmembrane helices in the open state of P2X receptor channels. *Proc Natl Acad Sci U S A* **110**, E4045–4054.

Jindrichova M, Vavra V, Obsil T, Stojilkovic SS & Zemkova H (2009). Functional relevance of aromatic residues in the first transmembrane domain of P2X receptors. *J Neurochem* **109**, 923–934.

Kawate T, Michel JC, Birdsong WT & Gouaux E (2009). Crystal structure of the ATP-gated P2X4 ion channel in the closed state. *Nature* **460**, 592–598.

Keceli B & Kubo Y (2009). Functional and structural identification of amino acid residues of the P2X2 receptor channel critical for the voltage- and [ATP]-dependent gating. *J Physiol* **587**, 5801–5818.

Keceli B & Kubo Y (2014). Signal transmission within the P2X2 trimeric receptor. *J Gen Physiol* **143**, 761–782.

Khakh BS (2001). Molecular physiology of P2X receptors and ATP signalling at synapses. *Nat Rev Neurosci* **2**, 165–174.

Khakh BS & North RA (2006). P2X receptors as cell-surface ATP sensors in health and disease. *Nature* **442**, 527–532.

Khakh BS & North RA (2012). Neuromodulation by extracellular ATP and P2X receptors in the CNS. *Neuron* **76**, 51–69.

Kiefer F, Arnold K, Kunzli M, Bordoli L & Schwede T (2009). The SWISS-MODEL Repository and associated resources. *Nucleic Acids Res* **37**, D387–392.

Kubo Y, Fujiwara Y, Keceli B & Nakajo K (2009). Dynamic aspects of functional regulation of the ATP receptor channel P2X2. *J Physiol* **587**, 5317–5324.

Li M, Chang TH, Silberberg SD & Swartz KJ (2008). Gating the pore of P2X receptor channels. *Nat Neurosci* **11**, 883–887.

Li M, Kawate T, Silberberg SD & Swartz KJ (2010). Pore-opening mechanism in trimeric P2X receptor channels. *Nat Commun* **1**, 44.

Narula SS, Brouwer M, Hua Y & Armitage IM (1995). Three-dimensional solution structure of Callinectes sapidus metallothionein-1 determined by homonuclear and heteronuclear magnetic resonance spectroscopy. *Biochemistry* **34**, 620–631.

Naylor CE, Eaton JT, Howells A, Justin N, Moss DS, Titball RW & Basak AK (1998). Structure of the key toxin in gas gangrene. *Nat Struct Biol* **5**, 738–746.

North RA (2002). Molecular physiology of P2X receptors. *Physiol Rev* **82**, 1013–1067.

Nour-Eldin HH, Geu-Flores F & Halkier BA (2010). USER cloning and USER fusion: the ideal cloning techniques for small and big laboratories. *Methods Mol Biol* **643**, 185–200.

Ohana L, Barchad O, Parnas I & Parnas H (2006). The metabotropic glutamate G-protein-coupled receptors mGluR3 and mGluR1a are voltage-sensitive. *J Biol Chem* **281**, 24204–24215.

Raghuraman H, Cordero-Morales JF, Jogini V, Pan AC, Kollewe A, Roux B & Perozo E (2012). Mechanism of Cd^{2+} coordination during slow inactivation in potassium channels. *Structure* **20**, 1332–1342.

Roberts JA, Allsopp RC, El Ajouz S, Vial C, Schmid R, Young MT & Evans RJ (2012). Agonist binding evokes extensive conformational changes in the extracellular domain of the ATP-gated human P2X1 receptor ion channel. *Proc Natl Acad Sci U S A* **109**, 4663–4667.

Rulisek L & Vondrasek J (1998). Coordination geometries of selected transition metal ions (Co^{2+}, Ni^{2+}, Cu^{2+}, Zn^{2+}, Cd^{2+}, and Hg^{2+}) in metalloproteins. *J Inorg Biochem* **71**, 115–127.

Stelmashenko O, Lalo U, Yang Y, Bragg L, North RA & Compan V (2012). Activation of trimeric P2X2 receptors by fewer than three ATP molecules. *Mol Pharmacol* **82**, 760–766.

Yellen G, Sodickson D, Chen TY & Jurman ME (1994). An engineered cysteine in the external mouth of a K+ channel allows inactivation to be modulated by metal binding. *Biophys J* **66**, 1068–1075.

Zhou Z & Hume RI (1998). Two mechanisms for inward rectification of current flow through the purinoceptor P2X2 class of ATP-gated channels. *J Physiol* **507**, 353–364.

Additional information

Competing interests

There are no competing interests.

Author contributions

B.K. and Y.K. designed research. B.K. performed experiments and analysed data. B.K. and Y.K. wrote the manuscript.

Funding

This work was supported in part by research grants from the Japan Society for Promotion of Science to B.K. and to Y.K.

Acknowledgements

We would like to thank Dr D. Julius (University of California, San Francisco) for providing us with P2X2 cDNA. We also thank Dr Y. Fujiwara (Osaka University) for discussion, Dr K. Nakajo and other Kubo Lab members for discussion and comments, Ms Y. Asai and Ms C. Naito for technical assistance, and Dr A. Collins (Queen's University Belfast) for comments and text editing.

Author's present address

Batu Keceli: Department of Neuroscience, University of Texas Southwestern Medical Center, 5323 Harry Hines Blvd, Dallas, TX 75390-9111, USA. Email: Batu.Keceli@UTSouthwestern.edu